Changes of "brain-GI" interplay in Parkinson's disease: a pilot study of dynamic total-body [11C]CFT PET/CT and kinetic modeling

Mei Xin[1], Yihan Wang[2], Xinlan Yang[2], Lianghua Li[1], Cheng Wang[1], Yue Gu[2], Chenpeng Zhang[1], Gang Huang[1], Yun Zhou[2], and Jianjun Liu[1]

[1]Shanghai Jiao Tong University School of Medicine Affiliated Renji Hospital
[2]Central Research Institute, United Imaging Healthcare Group Co, Ltd, Shanghai, China.

September 6, 2023

Abstract

Purpose: Parkinson's disease (PD) is a neurodegenerative disease characterized by progressive loss of dopaminergic neurons in the brain. To achieve better explorations of dopamine changes both centrally and peripherally, we employed uEXPLORER dynamic [11C]CFT PET/CT imaging combined with voxel-wise kinetic modeling. Methods: Eleven participants (five patients, PD and six healthy volunteers, HC) underwent 75-min dynamic scans were enrolled. Volumes of interest for four nigrostriatal nuclei (caudate, putamen, pallidum and substantial nigra) and three digestive organs (pancreas, stomach and duodenum) were delineated. Total-body parametric images of relative transporter rate constant (R1) and distribution volume ratio (DVR) using the simplified reference tissue model (SRTM2) were quantitatively generated by a linear regression with spatial-constraint algorithm. Standardized uptake value ratio (SUVR) at early and late phase were calculated as the semi-quantitative substitutes. Results: Significant differences between the two groups were identified in DVR and SUVRLP of putamen ($P < 0.05$) and SUVREP of stomach ($P < 0.01$). For HC group, negative correlations of R1 were achieved between stomach and both putamen and substantial nigra (all $P < 0.05$); positive correlations of DVR were identified between pancreas and all four brain nuclei (all $P < 0.05$). Yet in PD group, correlations of R1 or DVR between the targeted digestive and brain areas were considerably diminished. Similar trends in correlations were also found in SUVR analysis. Conclusions: We introduced a pioneering approach using dynamic total-body [11C]CFT PET/CT imaging to investigate distinctive patterns of potential "brain-GI" interplays, which may provide new insights towards the understanding of PD.

Changes of "brain-GI" interplay in Parkinson's disease: a pilot study of dynamictotal-body [^{11}C]CFT PET/CT and kinetic modeling

Running title: Total-body PET on "brain-GI" interplay

Mei Xin [1+], Yihan Wang [2+], Xinlan Yang [2], Lianghua Li [1], Cheng Wang [1], Yue Gu[2], Chenpeng Zhang [1], Gang Huang[1], Yun Zhou [2*], Jianjun Liu[1*]

[1] Department of Nuclear Medicine, Renji Hospital, Shanghai Jiao Tong University School of Medicine, Shanghai 200127, China

[2] Central Research Institute, United Imaging Healthcare Group Co, Ltd, Shanghai 201807, China.

[+] **These authors contribute equally to the article.**

*** Corresponding Authors** : **Yun Zhou** , 2258 Chengbei Road, Shanghai 201807, China, Tel: 862167076888, Fax: 862167076889, Email: yun.zhou@united-imaging.com; **Jianjun Liu** , 160 Pujian Road, Shanghai 200127, China, Tel: 862168383098, Fax: none, Email: nuclearj@163.com

Conflict of interest : All authors declare that they have no conflict of interest.

Funding : This work was supported by the National Key Research and Development Program of China (Grant number 2021YFA0910000), and the National Natural Science Foundation of China (Grant number 82171972).

Abstract

Purpose: Parkinson's disease (PD) is a neurodegenerative disease characterized by progressive loss of dopaminergic neurons in the brain. To achieve better explorations of dopamine changes both centrally and peripherally, we employed uEXPLORER dynamic [^{11}C]CFT PET/CT imaging combined with voxel-wise kinetic modeling.

Methods: Eleven participants (five patients, PD and six healthy volunteers, HC) underwent 75-min dynamic scans were enrolled. Volumes of interest for four nigrostriatal nuclei (caudate, putamen, pallidum and substantial nigra) and three digestive organs (pancreas, stomach and duodenum) were delineated. Total-body parametric images of relative transporter rate constant (R_1) and distribution volume ratio (DVR) using the simplified reference tissue model (SRTM2) were quantitatively generated by a linear regression with spatial-constraint algorithm. Standardized uptake value ratio (SUVR) at early and late phase were calculated as the semi-quantitative substitutes.

Results: Significant differences between the two groups were identified in DVR and $SUVR_{LP}$ of putamen ($P< 0.05$) and $SUVR_{EP}$ of stomach ($P< 0.01$). For HC group, negative correlations of R_1 were achieved between stomach and both putamen and substantial nigra (all $P < 0.05$); positive correlations of DVR were identified between pancreas and all four brain nuclei (all$P < 0.05$). Yet in PD group, correlations of R_1 or DVR between the targeted digestive and brain areas were considerably diminished. Similar trends in correlations were also found in SUVR analysis.

Conclusions: We introduced a pioneering approach using dynamic total-body [^{11}C]CFT PET/CT imaging to investigate distinctive patterns of potential "brain-GI" interplays, which may provide new insights towards the understanding of PD.

Key words: Total-body PET/CT; Parkinson's disease; "Brain-GI" interplay; [^{11}C]CFT; Parametric imaging

Introduction

Parkinson's disease (PD) is a progressive neurodegenerative disorder common in elderly population that increases in prevalence with age. The principal pathophysiological change of PD lies in the depletion of nigrostriatal dopaminergic neurons, leading to a series of motor symptoms including bradykinesia, tremor, rigidity and gait instability[1]. With the broaden understanding of the disease timeline, both the "brain-first" or "body-first" etiologic hypotheses emphasize on the integrity of the organism and the interactions between the central and peripheral nerve systems, particularly in relation to the gastrointestinal (GI) organs[2]. Widely distributed across the GI tract, the enteric nerve system (ENS), termed as "the second brain", accounts for the largest division of the peripheral nerve system [3, 4]. Recent studies have suggested that the communication between the brain and digestive systems may be mediated by certain agents present in both areas, potentially influencing the disease occurrence, development, and modulation[5].

Dopamine transporter (DAT) is a neurotransmitter protein on the presynaptic membrane that is responsible for the reuptake of extracellular dopamine (DA) from the synaptic cleft and regulates the DA neurotransmission and homeostasis. Besides the nigrostriatal pathway within the brain, the expression of DAT can also be found at several peripheral sites [6], and in turn influences numerous peripheral functions including gastrointestinal motility, functioning in a variety of neuropsychiatric disorders in PD. Immunohistochemical and in situ hybridization studies indicated that DATs are abundantly expressed in the GI track, including the two important nerve branches – Meissner's and Auerbach's plexuses of the ENS, the gastric parietal cells and mucosal blood vessel endothelia, duodenal lamina propria, pancreatic excreting ducts and islets [7-10].

Several studies have also demonstrated the association between the striatal DAT binding and the activities of gut microbes, suggesting DAT modulations through the "brain-GI" axis[11, 12].

However, few suitable approaches are available to make a systemic and quantitative analysis of DAT kinetic distribution in both the central and peripheral organs of human. Nowadays, progress has been made to understand the etiology of neurodegenerative diseases at molecular level with the visualization of the imaging biomarkers. The most widely accessible imaging approach is the use of PET or SPECT tracers for the DAT targets.^{11}C-2-beta-carbomethoxy-3-beta-(4-fluorophenyl)tropane ([^{11}C]CFT), a mature DAT positron imaging agent, has been commonly used in brain imaging for the diagnosis of PD[13-15]. Moreover , in animal models, highly specific uptakes of DAT radioligand [^{18}F]CFT have been demonstrated in both the striatum and pancreas with the treatment of selective DAT antagonist[16], showing the potential of radionuclide-labeled CFT compound used to evaluate the interplay between the central and GI regions. Meanwhile, breaking through the technical limitations from the standard PET/CT with multi-beds scanning, the super-high temporal-spatial resolution and 194 cm-super-long axial field of view (AFOV) total-body PET/CT enables us to track the dynamic changes of the internal tracer distribution in a real-time and quantitative way[17-19]. Precise time-activity curves (TACs) enables the simultaneous study of the kinetic interplay between organs, which may lead to better understanding of coordination between the brain function and other physiological activities [20]. Compared to the conventional a-priori volume of interest (VOI) kinetic analysis approach, the parametric imaging offers additional quantitative values into varied pathophysiological alterations, which may emerge as a standard for visualizing pathophysiology, diagnosing, monitoring neurodegenerative disease progression, and assessing therapeutic outcomes [21].

In this study, we employed two image-based methods to measure the total-body dynamic [^{11}C]CFT kinetics between the PD patients and healthy volunteers – the quantitative analysis using a simplified reference tissue model (SRTM2) and the semi-quantitative measurement based on the standardized uptake value ratio (SUVR). Based on the novel technical platform of dynamic [^{11}C]CFT total-body PET/CT imaging, our study aimed to explore the potential variation and correlations in the tracer kinetics between the selected brain and GI regions.

Methods

Participants

Eleven participants including five untreated patients diagnosed as PD (PD group) and six healthy volunteers as controls (HC group) underwent [^{11}C]CFT total-body PET/CT scans in our department from January to December 2021. The neurologic assessment for patients including the third part of Unified Parkinson Disease Rating Scale (UPDRS III), modified Hoehn and Yahr stage (mH-Y), and Non-motor Symptoms Scale (NMSS) were recorded. The detailed characteristics of all participants were listed in **Table 1** . Healthy volunteers were sourced from health screening participants with no history of significant medical, neuropsychiatric illnesses, or neoplastic diseases, which were excluded using [^{18}F]FDG PET/CT. This retrospective study followed the principles of the Declaration of Helsinki and has been approved by the ethics committee of Renji Hospital with written informed consent waived.

Radiopharmaceutical Preparation

The radionuclide, $^{11}CO_2$, was prepared by the medical cyclotron (HM-10, Sumitomo) in our department. [^{11}C]CFT was produced by an automatic synthesis module (CFN-MPS-200, Sumitomo) according to the previously reported method[22]. The radiochemical purity of [^{11}C]CFT was above 95%.

Dynamic Total-Body PET/CT Acquisition and Reconstruction

All participants underwent dynamic [^{11}C]CFT PET imaging using a total-body PET/CT scanner (uEXPLORER, United Imaging Healthcare). CT images were collected from vertex to toes for attenuation correction prior to PET acquisition. A 75-min PET scan was performed on each participant immediately after a lower limb intravenous bolus injection of 431.4±75.6 MBq ^{11}C-CFT. The dynamic PET images were corrected for radioactive decay, scatter, attenuation, and random, and were reconstructed into a matrix

with voxel size of 2.34 ×2.34×2.89 mm^3 in x, y, z direction with ordered subset expectation maximization (OSEM) algorithm, time-of-flight (TOF) and point-spread function (PSF). The images were split into 97 frames (30×2 s, 12×5 s, 6×10 s, 4×30 s, 25×60 s, 15×120 s, 5×180 s)[23, 24].

Dynamic PET Image Processing

VOIs were manually drawn within descending aorta, duodenum, pancreas, and stomach using PMOD 4.3 software (PMOD Technologies Ltd.), where the descending aorta was selected to reflect the blood radiotracer concentration. To extract the TACs from the brain regions, all PET images were first processed by head motion correction and spatial normalization, both using Statistical Parametric Mapping software (SPM12, Wellcome Department of Imaging Neuroscience) in the MATLAB (2019b, The MathWorks Inc.) environment, followed by the co-registration of the PET images to the standard Montreal Neurologic Institute (MNI) space based on an MRI template[25]. Caudate, putamen, pallidum, and substantial nigra, which are the major brain regions associated with PD, were selected for the analysis. TACs of all organs were then extracted for kinetic analysis. The mean standardized uptake value (SUV_{mean}) curves, which can be calculated as the average radioactivity within each VOI at each frame normalized by the ratio between the decay-corrected injected radiolabeled dose and body weight of the participant, were generated based on the TACs. In the SUV_{mean} curve analysis of the brain nuclei, the separation time was calculated as the time when the difference in group means between the SUV_{mean} of HC and PD reached to at least 10% of the mean SUV_{mean} of HC group.

Reference Tissue-based Kinetic Modeling

The SRTM2 was used for the voxel-wise [^{11}C]CFT kinetic analysis[21, 26, 27], which generated two parametric images: R_1 (the ratio between the transport rate constants of target and reference tissues) and DVR (distribution volume ratio between the target and reference tissues). The R_1 represents the relative transporter rate constant of tracer from vascular space to the target organs or brain regions, whereas DVR reflects the tracer specific binding to DAT. The occipital lobe region lacking DAT distribution was selected as the reference tissue. A linear regression with spatial constraint algorithm was used to generate parametric images of R_1 and DVR[21, 28].

To the best of our knowledge, no clinical studies have yet conducted a total-body dynamic [^{11}C]CFT analysis utilizing the voxel-wise SRTM2 method. Thus, we additionally performed the VOI-based one-tissue compartmental modeling (1T2K) with the metabolite-corrected TAC of descending aorta as the input function using PMOD to validate our SRTM2 estimates [28]. The tracer transport rate constant (K_1) and total distribution volume (V_T) as the estimates for early blood perfusion and later tracer density were generated to validate the use of R_1 and DVR, respectively.

Kinetic Analysis with Semi-Quantification Approach

SUVR, calculated as the ratio between the SUV of the targeted area and occipital lobe reference region, served as an approximation of early blood perfusion and DAT expression level with an advantage of shorter scan acquisition time for clinical setting. The whole dynamic scanning period of [^{11}C]CFT was subdivided into the early phase ($SUVR_{EP}$ for 1-3 min) and late phase ($SUVR_{LP}$ for 60-75 min), where $SUVR_{EP}$ was used to estimate R_1 and $SUVR_{LP}$ can be used as an approximation of the tracer specific binding to DAT resembling DVR [21].

Statistical Analysis

All statistical analysis were performed using R (version 4.2.0) and GraphPad (version 9.0) software. The descriptive data of SUV_{mean} curve characteristics and quantification estimates were presented as mean (standard deviation, SD). Pearson's correlation analysis was used to compare the relationship between the targeted areas, as well as assessing the agreement between the estimates generated by different approaches. $P < 0.05$ was considered statistically significant.

Results

Total-body dynamic [^{11}C]CFT PET Imaging

The schematic PET/CT acquisition protocol, representative maximum intensity projection (MIP) images, and the transverse views of cerebral nuclei and GI organs acquired at different time points were shown in**Figure 1** . In the total-body dynamic [^{11}C]CFT PET imaging, the tracer uptake in the central and peripheral regions throughout the entire body were clearly visualized, even in deep brain areas like the substantial nigra, which was usually limited by resolution with conventional PET scanner. Based on the visual assessment, the uptake of [^{11}C]CFT in the nigrostriatal nuclei of HC is intact and persistent, while PD patients displayed asymmetric DAT depletion in the corresponding areas. No distinct difference was observed from the visual assessment of GI organ regions between the HC and PD groups.

Characterization of SUV_{mean} curve

The SUV_{mean} curves of descending aorta and occipital lobe in the HC and PD groups were depicted in **Figure 2A** and**B** , demonstrating negligible difference in curve pattern of both regions between the two groups. As the time went on, the ascending curves of the brain nuclei in the two groups started to separate: while the [^{11}C]CFT uptake of HC group kept increasing, the uptake of PD group tended to reach the "plateau" in advance (**Figure 2C , Table 2**). In putamen, [^{11}C]CFT uptake of the two groups first showed an early distinction (separation time = 2 min), and the statistical significance was found in the highest SUV_{mean} between the two groups (P <0.05).

The SUV_{mean} curve patterns of the pancreas and duodenum could be characterized as "fast-in and slow-out" in both groups, where the peak activities of the HC group in these two organs were higher than the PD group. In the stomach, a relatively faster rising uptake in PD patients was observed in the early stage, yet the final SUV_{mean} of the HC group at 75 min appeared to be higher (**Figure 2D** and **Table 2)** .

Kinetic analysis features

The total-body [^{11}C]CFT PET parametric images based on the SRTM2 model were generated. The schematic formula of SRTM2 and representative R_1 and DVR parametric images of HC and PD participants were illustrated in **Figure 3A** and**B** . The statistically significant correlation was observed between the parameters of quantitative and semi-quantitative analysis, including R_1 and $SUVR_{EP}$ (r =0.776,P <0.001), DVR and $SUVR_{LP}$(r =0.921,P <0.001), suggesting an agreement between the two analysis approaches (**Figure 3C**). In the comparison of the quantitative parameters between HC and PD groups, statistical significances were found between the HC and PD groups in terms of $SUVR_{EP}$ of stomach (P <0.01) and both DVR and $SUVR_{LP}$of putamen (P <0.05) (**Figure 3D**).

We further demonstrated that the R_1 and DVR estimated from the SRTM2 using the occipital lobe as the reference was highly correlated with the K_1 and V_T generated from the 1T2K models (r = 0.84 and 0.83, respectively, both$P$ <0.0001) (**Supplemental Figure 1A** and**B**), suggesting the accurate tracer quantification without arterial sampling.

Correlations between the specific brain nuclei and GI organs

Pairwise comparisons within the digestive and cerebral regions of the HC and PD group were separately summarized (**Figure 4-5**). For the inter-nigrostriatal region correlations, strong positive correlation for R_1, DVR, $SUVR_{EP}$ and $SUVR_{LP}$ were found among nearly all the four nigrostriatal nuclei within the HC group (all P <0.05). Conversely, these correlations were notably diminished in the PD cohort.

For the "brain-GI" correlations within the HC group, the significant negative correlations were revealed between the stomach and putamen for both the early perfusion parameters R_1 (r =-0.833, P <0.05) and $SUVR_{EP}$ (r =-0.821, P <0.05). Meanwhile, the significant positive correlation relationships of the tracer density parameters DVR and $SUVR_{LP}$ were identified between pancreas and all the four brain nuclei including caudate (r =0.918, P <0.05 for DVR; r =0.899,P <0.05 for $SUVR_{LP}$), putamen (r =0.977, P <0.001 for DVR; r =0.993,P <0.001 for $SUVR_{LP}$), pallidum (r =0.909, P <0.05 for DVR; r =0.828,P <0.05 for $SUVR_{LP}$) and substantial nigra (r =0.894, P <0.05 for DVR; r =0.964,P <0.01 for $SUVR_{LP}$). In contrast,

among PD patients, significant correlations between most of the brain nuclei and digestive organ targets were absent, except for a positive correlation was observed between the pancreas and pallidum (r=0.912, P <0.05 for DVR; r =0.904,P <0.05 for $SUVR_{LP}$), and substantia nigra (r =0.912, P <0.05 for $SUVR_{LP}$). Additionally, the V_T of pancreas and putamen estimated using the VOI-based 1T2K were also significantly correlated in the HC group rather than PD group (**Supplemental Figure 1C**).

Discussion

Since discovered 200 years ago, the practice of exploring PD has never stopped. According to the various and systemic symptoms of PD populations, herein we attempted to break out the limitation of single studies confined to the brain, with the application of [^{11}C]CFT tracer targeting DAT and advantages of the integrated dynamic total-body PET/CT imaging, aimed to systematically evaluate the potential patterns related to the dopaminergic changes and interactions among the digestive and cerebral regions. Dopamine serves as a protective agent for human GI system, preventing gastric and intestinal mucosa from injury, resisting against peptic ulcer, and promoting ulcer healing[29]. PD patients also have a relatively high incidence of duodenal ulcers, while the GI dysfunction or dysmotility are often likely due to the DA deficiency or peripheral DAT depletion[30]. Most of the previous reports on DA and DAT focused on their neurotransmitter function only in the central nerve system (CNS). However, certain peripheral organs also have abundant DAT expression. Recent studies have indicated that at the time when pathological α-synuclein aggregation was found in the submucosal and myenteric neurons, there also existed abnormal changes of dopaminergic neurons in these enteric plexuses both in PD patients and animal models[31-33]. However, it is unknown whether peripheral DAT uptake capacity and/or its level are changed. A potential relationship between peripheral and central DAT may assess the disease progression and the effectiveness of pharmacotherapies in PD[34]. Therefore, it is necessary to employ a macroscopic, whole-body approach to make an integrated evaluation of the DA signaling and homeostasis both in the CNS and ENS.

From the SUV_{mean} curve analysis of the cerebral core areas (caudate, putamen, pallidum and substantial nigra), the tracer activities of the four nuclei in healthy volunteers continuously increased over time, suggesting the integrity of the dopaminergic function of the nigrostriatal system in healthy brains. Moreover, the strong positive correlations between the quantitative parameters among these brain nuclei also yielded similar network connections. Instead, the [^{11}C]CFT uptakes of the targeted nuclei in PD patients tended to approach the "plateau" in advance, especially in the putamen with the earlier occurrence of dopamine loss. This is in accordance with the caudal-rostral gradient rule of striatal dopamine depletion in the disease progress. In the pancreas and duodenum, the peak [^{11}C]CFT activity of healthy participants was higher than that of the patients, indicating a potential peripheral dopaminergic neuron impairment in these two regions that may be related to PD. In the stomach, due to the natural peristole influence of this motional organ, resulted in a consistent fluctuation of the SUV_{mean} curve over time. Despite this, the final tracer uptake remained higher in the healthy volunteers, suggesting a potential binding reduction of the stomach in PD patients.

The quantitative method incorporated with kinetic modeling provides direct information on the specific biologic process, representing the tissue density of DAT and relative transporter rate constant of the tracer , whereas the semi-quantitative method of SUVR requires shorter scan acquisition and thus is often favored in clinical setting to estimate such parameters[21]. Our prior study found certain correlations between the pancreas, duodenum, stomach and the nigrostriatal nuclei in the healthy participants rather than PD patients in the correlation analysis based on [^{11}C]CFT total-body dynamic PET/CT imaging with SUV_{mean} measurements for the "brain-GI" targeted areas[35]. In this study, we further introduced voxel-based quantitative analysis based on SRTM2 modeling together with the SUVR semi-quantitative analysis to explore the interplay between the digestive and cerebral regions. For the healthy population, there was a negative correlation of the relative blood perfusion estimate R_1 between stomach and the certain brain nuclei, whereas in terms of the DAT density estimate DVR, the significant positive correlation between pancreas and the specific brain nuclei were also demonstrated. In addition, both the semi-quantitative estimates, $SUVR_{EP}$ and $SUVR_{LP}$, indicated similar correlation results from the quantification approach in most of the region pairs.

This indicated that there may exist an original intrinsic correlation upon the "brain-GI" neuronal chain in healthy individuals rather than the PD patients. Previous research on animal models of DAT specific SPECT tracers (^{99m}Tc-TRODAT-1) suggested specific high uptakes in the gastric mucosa [36]. Herein the correlation relationship between the stomach and core brain nuclei probably may attribute to the early perfusion of the tracer from the gastric mucosal vascular epithelium. Huang et al.[37] found a high pancreas uptake by using standard [^{11}C]CFT PET/CT in healthy individuals. The correlation discrepancies between the HC and PD groups in our findings indicated the native "healthy" interplay pattern related to the digestive and cerebral dopaminergic interaction might be diminished with the disease occurrence.

The simplified reference region model demonstrated a higher computational efficiency and voxel-level stability compared to that of nonlinear least squares method in describing the kinetic of [^{11}C]CFT in rats, suggested by Gunn et al.[27]. Other advantages of the SRTM2 method also include the avoidance of arterial cannulation and metabolite measurements[38]. As the compartmental modeling approach with plasma input are usually considered the "gold standard" in kinetic analysis, we additionally performed the VOI-based 1T2K kinetic modeling to verify the estimates from the SRTM2[21, 26, 27, 38]. The results of the highly correlated DVR estimated from SRTM2 using the occipital lobe as the reference and the V_T generated from the 1T2K models suggested the accurate tracer quantification without arterial sampling. The significant correlation in V_T of pancreas and putamen in the HC group rather than PD group was consistent to the results represented by DVR and $SUVR_{LP}$, providing more evidence towards the interplay alteration due to the PD occurrence.

Using the correlation analysis between the brain nuclei and digestive organs is a primary attempt to investigate the complex interplay between the digestive and cerebral regions in PD based on noninvasive molecular imaging. Prospective studies with more participants and more records of GI symptoms will be needed to confirm the findings. Since long scanning time in dynamic PET/CT acquisition may be challenging for the PD patients, our results on the high consistency between the quantitative and semi-quantitative estimates will support the semi-quantitative measurements to be the potential surrogates for estimating tracer kinetics with shorter scanning time, facilitating the participant recruitment in the future prospective studies. Moreover, several image-based systematic approaches in brain analysis have been applied to the study of organ-level total-body metabolic network of rodent[39], which may have potential prospect in the interpretation of PD etiology and disease evaluation in the clinical practice.

Conclusion

With the pilot application of the dynamic total-body [^{11}C]CFT PET/CT imaging along with the quantitative and semi-quantitative approaches, we observed the distinctive uptake patterns in correlative interplays between the digestive and cerebral regions of HC and PD, which may provide new insights towards the understanding of disease.

Reference

1. L. V. Kalia and A. E. Lang,*The Lancet* , 2015, **386** , 896-912.

2. J. Horsager, K. B. Andersen, K. Knudsen, C. Skjaerbaek, T. D. Fedorova, N. Okkels, E. Schaeffer, S. K. Bonkat, J. Geday, M. Otto, M. Sommerauer, E. H. Danielsen, E. Bech, J. Kraft, O. L. Munk, S. D. Hansen, N. Pavese, R. Goder, D. J. Brooks, D. Berg and P. Borghammer, *Brain : a journal of neurology* , 2020,**143** , 3077-3088.

3. R. A. Liddle, *Brain research* , 2018, **1693** , 201-206.

4. A. Chalazonitis and M. Rao,*Brain research* , 2018, **1693** , 207-213.

5. A. Adamantidis, *Science* , 2022, **376** , 248-249.

6. B. E. Tóth, M. Vecsernyés, T. Zelles, K. Kádár and G. M. Nagy, *Advances in Neuroimmune Biology* , 2012, **3** , 111-155.

7. T. Mitsuma, H. Rhue, Y. Hirooka, M. Kayama, T. Wago, J. Takagi, K. Adachi, J. Ping, M. Ohtake, T. Nogimori and J. Sakai, *Endocrine regulations* , 1998, **32** , 71-75.

8. G. Eisenhofer, *Pharmacology & therapeutics* , 2001, **91** , 35-62.

9. Y. M. Tian, X. Chen, D. Z. Luo, X. H. Zhang, H. Xue, L. F. Zheng, N. Yang, X. M. Wang and J. X. Zhu,*Neuroscience* , 2008, **153** , 634-644.

10. A. Ustione and D. W. Piston,*Molecular endocrinology* , 2012, **26** , 1928-1940.

11. S. Hamamah, A. Aghazarian, A. Nazaryan, A. Hajnal and M. Covasa, *Biomedicines* , 2022,**10** .

12. A. V. Hartstra, V. Schuppel, S. Imangaliyev, A. Schrantee, A. Prodan, D. Collard, E. Levin, G. Dallinga-Thie, M. T. Ackermans, M. Winkelmeijer, S. R. Havik, A. Metwaly, I. Lagkouvardos, A. Nier, I. Bergheim, M. Heikenwalder, A. Dunkel, A. J. Nederveen, G. Liebisch, G. Mancano, S. P. Claus, A. Benitez-Paez, S. E. la Fleur, J. J. Bergman, V. Gerdes, Y. Sanz, J. Booij, E. Kemper, A. K. Groen, M. J. Serlie, D. Haller and M. Nieuwdorp,*Molecular metabolism* , 2020, **42** , 101076.

13. S. Zhu, Z. Ju, P. Wu, F. Liu, J. Ge, H. Zhang, J. Lu, L. Li, M. Wang, J. Jiang, J. Wang and C. Zuo,*Behavioural neurology* , 2021, **2021** , 2230196.

14. X. Sun, F. Liu, Q. Liu, Y. Gai, W. Ruan, D. N. Wimalarathne, F. Hu, X. Tan and X. Lan, *Frontiers in neuroscience* , 2019, **13** , 299.

15. F. T. Liu, J. J. Ge, J. J. Wu, P. Wu, Y. Ma, C. T. Zuo and J. Wang, *Clinical nuclear medicine* , 2018, **43** , 562-571.

16. S. Forsback, P. Marjamaki, O. Eskola, J. Bergman, J. Rokka, T. Gronroos, M. Haaparanta and O. Solin,*EJNMMI research* , 2012, **2** , 3.

17. R. D. Badawi, H. Shi, P. Hu, S. Chen, T. Xu, P. M. Price, Y. Ding, B. A. Spencer, L. Nardo, W. Liu, J. Bao, T. Jones, H. Li and S. R. Cherry, *J Nucl Med* , 2019,**60** , 299-303.

18. B. A. Spencer, E. Berg, J. P. Schmall, N. Omidvari, E. K. Leung, Y. G. Abdelhafez, S. Tang, Z. Deng, Y. Dong, Y. Lv, J. Bao, W. Liu, H. Li, T. Jones, R. D. Badawi and S. R. Cherry, *Journal of nuclear medicine : official publication, Society of Nuclear Medicine* , 2021, **62** , 861-870.

19. X. Zhang, S. R. Cherry, Z. Xie, H. Shi, R. D. Badawi and J. Qi, *Proceedings of the National Academy of Sciences of the United States of America* , 2020,**117** , 2265-2267.

20. L. Nardo, J. P. Schmall, T. J. Werner, M. Malogolowkin, R. D. Badawi and A. Alavi, *PET clinics* , 2020, **15** , 271-279.

21. Y. Zhou, S. Flores, S. Mansor, R. C. Hornbeck, Z. Tu, J. S. Perlmutter, B. Ances, J. C. Morris, R. J. Gropler and T. L. S. Benzinger, *European journal of nuclear medicine and molecular imaging* , 2021, **48** , 3172-3186.

22. G. Tang, X. Tang, H. Deng, H. Wang, F. Wen, C. Yi and K. Wu, *Nuclear medicine communications* , 2011, **32** , 466-474.

23. R. Chen, X. Yang, Y. L. Ng, X. Yu, Y. Huo, X. Xiao, C. Zhang, Y. Chen, C. Zheng, L. Li, G. Huang, Y. Zhou and J. Liu, *Journal of nuclear medicine : official publication, Society of Nuclear Medicine* , 2023.

24. R. Chen, X. Yang, X. Yu, X. Zhou, Y. L. Ng, H. Zhao, L. Li, G. Huang, Y. Zhou and J. Liu, *Eur J Nucl Med Mol Imaging* , 2022.

25. Y. Li, Y. L. Ng, M. D. Paranjpe, Q. Ge, F. Gu, P. Li, S. Yan, J. Lu, X. Wang, Y. Zhou and I. for the Alzheimer's Disease Neuroimaging, *Human brain mapping* , 2022,**43** , 2121-2133.

26. Y. Zhou, C. J. Endres, J. R. Brasic, S. C. Huang and D. F. Wong, *NeuroImage* , 2003,**18** , 975-989.

27. R. N. Gunn, A. A. Lammertsma, S. P. Hume and V. J. Cunningham, *NeuroImage* , 1997, **6** , 279-287.

28. Y. Zhou, W. Ye, J. R. Brasic and D. F. Wong, *NeuroImage* , 2010, **49** , 2947-2957.

29. E. Mezey, G. Eisenhofer, G. Harta, S. Hansson, L. Gould, B. Hunyady and B. J. Hoffman,*Proceedings of the National Academy of Sciences of the United States of America* , 1996, **93** , 10377-10382.

30. E. Mezey, G. Eisenhofer, S. Hansson, B. Hunyady and B. J. Hoffman, *Neuroendocrinology* , 1998,**67** , 336-348.

31. C. Singaram, W. Ashraf, E. A. Gaumnitz, C. Torbey, A. Sengupta, R. Pfeiffer and E. M. Quigley,*Lancet* , 1995, **346** , 861-864.

32. G. Anderson, A. R. Noorian, G. Taylor, M. Anitha, D. Bernhard, S. Srinivasan and J. G. Greene,*Experimental neurology* , 2007, **207** , 4-12.

33. X. Li, W. Yang, X. Li, M. Chen, C. Liu, J. Li and S. Yu, *Neuroscience letters* , 2020,**716** , 134640.

34. P. Mackie, J. Lebowitz, L. Saadatpour, E. Nickoloff, P. Gaskill and H. Khoshbouei, *Brain, behavior, and immunity* , 2018, **70** , 21-35.

35. M. Xin, L. Li, C. Wang, Y. Wang, Y. Gu, C. Zhang, Y. Zhou and J. Liu, *Journal of Nuclear Medicine* , 2022, **63** , 2480-2480.

36. J. J. Hwang, M. H. Liao, T. C. Yen, S. P. Wey, K. J. Lin, W. H. Pan, J. C. Chen and G. Ting,*Applied radiation and isotopes : including data, instrumentation and methods for use in agriculture, industry and medicine* , 2002,**57** , 35-42.

37. T. Huang, H. Wang, G. Tang, X. Liang, H. Deng, C. Yi and X. Zhang, *Clin Nucl Med* , 2012,**37** , 1159-1162.

38. A. A. Lammertsma and S. P. Hume,*NeuroImage* , 1996, **4** , 153-158.

39. K. J. Suchacki, C. J. Alcaide-Corral, S. Nimale, M. G. Macaskill, R. H. Stimson, C. Farquharson, T. C. Freeman and A. A. S. Tavares, *Frontiers in medicine* , 2021, **8** , 740615.

Tables

TABLE 1. Patient Characteristics.

	Healthy volunteers as control (HC, n=6)	**Parkinson's disease patient (P**
Age, mean (SD), year	42 (15)	58 (8)
Weight, mean (SD), kg	67.0 (12.1)	78.6 (5.2)
Injected dose, mean (SD), MBq	418.8 (71.8)	443.8 (78.2)
UPDRS III, mean (SD)	N/A	16 (9)
mH-Y, mean (SD)	N/A	2 (1)
NMSS, mean (SD)	N/A	47 (48)

Abbreviation: UPDRS III, Unified Parkinson's Disease Rating Scale III; mH-Y, modified Hoehn and Yahr Scale; NMSS, Non-Motor Symptoms Scale.

TABLE 2. The SUV_{mean} curve characteristics of the target regions.

Uptake pattern	**Organs**	**Separation time, minute, minutes**	**Highest SUV_{mean}, m**
			HC
Gradually increasing	Caudate	6.5	7.2 (1.5)
	Putamen	2.0	8.6 (1.8)

Uptake pattern	Organs	Separation time, minute, minutes	Highest SUV_{mean}, m
	Pallidum	6.5	4.5 (1.2)
	SN	13.5	3.9 (0.7)
Increasing with fluctuation	Stomach	N/A	11.8 (5.0)
Rapid increasing and slow decreasing	Duodenum	N/A	5.3 (1.7)
	Pancreas	N/A	9.6 (3.2)

* $P < 0.05$.

Abbreviations: SD, standard deviation; HC, healthy control; PD, Parkinson's disease patient; SN, substantia nigra.

Figure Legends

FIGURE 1 (**A**)Total-body dynamic [^{11}C]CFT PET/CT scanning protocol (75 min, 97 frames). (**B-D**) Selected view from [^{11}C]CFT dynamic reconstructed images of a 53-year-old healthy volunteer (HC) and a 57-year-old Parkinson's disease patient (PD). (**B**) Total-body maximum intensity projection (MIP). (**C**) Transverse views of cerebral nuclei both in the striatal and substantial nigra plane. The [^{11}C]CFT uptake in HC developed earlier and increased over time, while the nigrostriatal dopamine depletion was finally found in PD with a caudal-rostral gradient tendency especially in the left side. (**D**) Transverse views of the upper abdomen. Abbreviation: HC, healthy controls; PD, Parkinson's disease patients.

FIGURE 2 Comparison of averaged SUV_{mean} curves in HC and PD group at the (**A**) descending aorta, (**B**)occipital lobe, selected (**C**) cerebral nuclei regions and (**D**) GI organs. Data are represented by mean ± standard error mean (SEM). Separation time between the averaged SUV_{mean}curves of HC and PD groups were marked for the cerebral nuclei regions.

FIGURE 3 (A) Schematic representation of the simplified reference tissue model (SRTM2). **(B)** Total-body maximum intensity projection (MIP) generated from the voxel-based SRTM2 modeling (left column), and representative striatal and substantial nigra planes of the R_1 and DVR parametric images in HC and PD representatives (right column). **(C)** Correlation between the quantitative and semi-quantitative measurements. The semi-quantitative estimation for early perfusion ($SUVR_{EP}$) (left) and dopamine transporter density ($SUVR_{LP}$) (right) were both significantly correlated to the quantitative parameters (R_1 and DVR, respectively).**(D)** Significant differences between the HC and PD groups in $SUVR_{EP}$ of stomach (left) and both DVR (middle) and $SUVR_{LP}$ (right) of putamen.

FIGURE 4 Correlative assessment of the **(A)**R_1 and **(B)** $SUVR_{EP}$ of stomach and substantial nigra, and the **(C)** DVR and **(D)**$SUVR_{LP}$ of pancreas and putamen in the HC and PD groups. Abbreviation: SN, substantia nigra

FIGURE 5 Correlation based on the quantitative measurements of (**A**) R_1 and (**B**) DVR, and semi-quantitative estimation of (**C**) $SUVR_{EP}$ and**(D)** $SUVR_{LP}$ between the cerebral nuclei and GI organs in healthy controls (HC) and Parkinson's disease patients (PD). Upper triangle gives the graphical demonstration of the correlation, where the orientations of the ellipses represent the signs of the correlation coefficient (upper-left to lower-right, negative; lower-left to upper-right, positive), and colors and width represent the magnitude of the coefficients. The asterisks represent the significance (*,P <0.05; **, P <0.01; ***,P <0.001). The lower triangle displays the correlation coefficient r . Abbreviation: SN, substantia nigra.

Figures

FIGURE 1

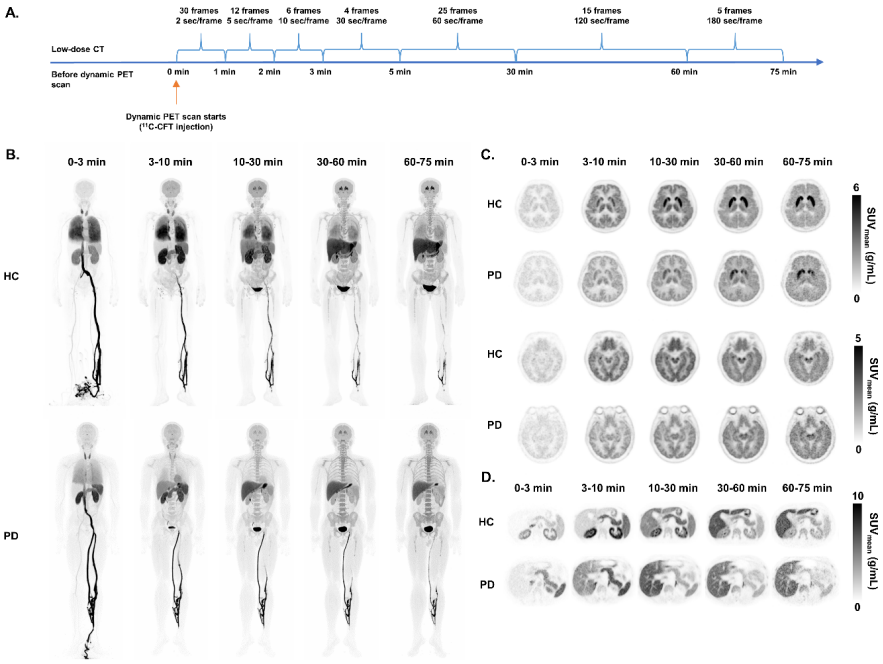

FIGURE 2

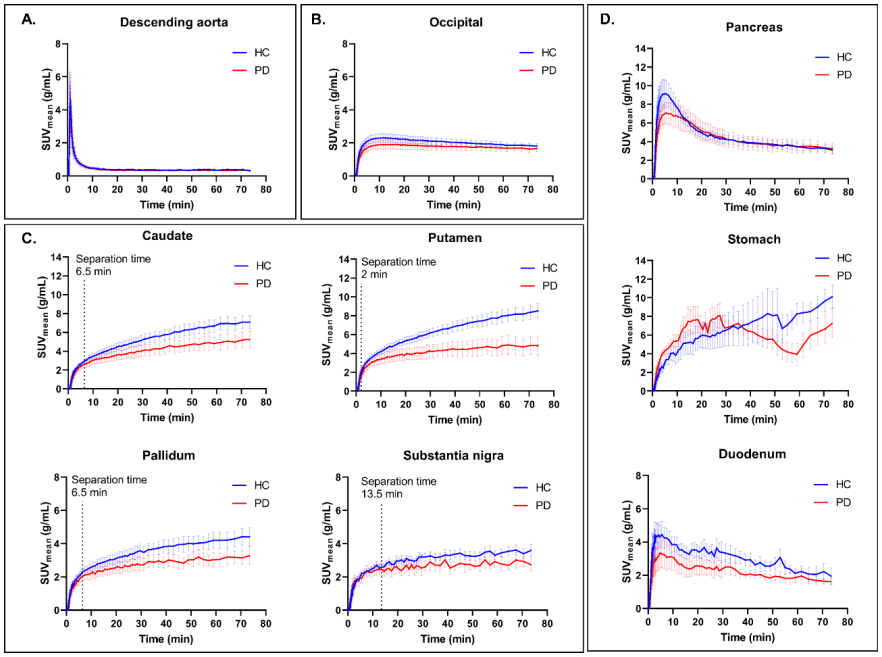

FIGURE 3

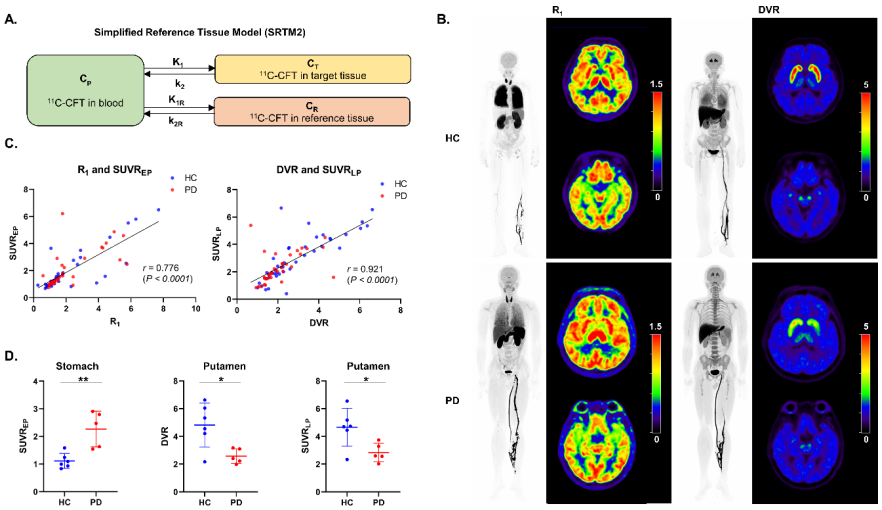

FIGURE 4

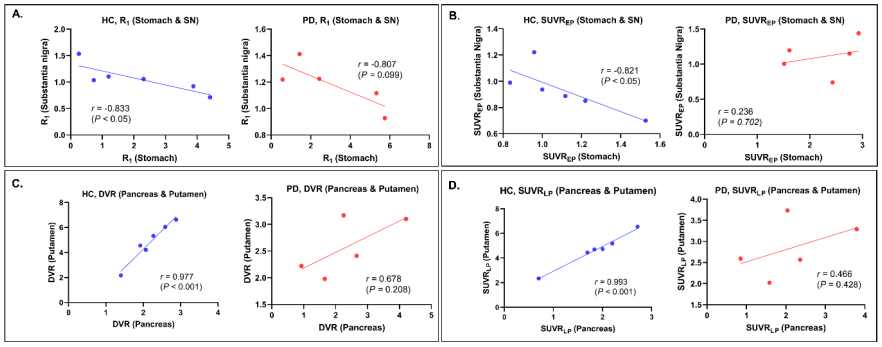

FIGURE 5